The Journal of Chemical Physics

RESEARCH ARTICLE | APRIL 04 2023

Photoelectron spectroscopy and dissociative photoionization of fulminic acid, HCNO

Marius Gerlach ; Barry Mant ; Tobias Preitschopf; Emil Karaev ; Dennis Mayer ; Heidy M. Quitián-Lara ; Patrick Hemberger ; John Bozek ; Graham Worth ; Ingo Fischer

J. Chem. Phys. 158, 134303 (2023)
https://doi.org/10.1063/5.0142194

AIP Publishing

The Journal of Chemical Physics ARTICLE scitation.org/journal/jcp

Photoelectron spectroscopy and dissociative photoionization of fulminic acid, HCNO

Cite as: J. Chem. Phys. 158, 134303 (2023); doi: 10.1063/5.0142194
Submitted: 12 January 2023 • Accepted: 13 February 2023 •
Published Online: 4 April 2023

Marius Gerlach,[1] Barry Mant,[2] Tobias Preitschopf,[1] Emil Karaev,[1] Dennis Mayer,[3] Heidy M. Quitián-Lara,[1,a)] Patrick Hemberger,[4] John Bozek,[5] Graham Worth,[2,b)] and Ingo Fischer[1,c)]

AFFILIATIONS

[1] Institute of Physical and Theoretical Chemistry, University of Würzburg, 97074 Würzburg, Germany
[2] Department of Chemistry, University College London, London WC1H 0AJ, United Kingdom
[3] Deutsches Elektronen-Synchrotron (DESY), 22607 Hamburg, Germany
[4] Laboratory for Synchrotron Radiation and Femtochemistry, Paul Scherrer Institut (PSI), 5232 Villigen, Switzerland
[5] Synchrotron SOLEIL, 91192 Gif-sur-Yvette, France

[a)] **Present address:** Centre for Astrophysics and Planetary Science (CAPS), School of Physics and Astronomy, University of Kent, Canterbury CT2 7NH, United Kingdom.
[b)] **Electronic mail:** g.a.worth@ucl.ac.uk
[c)] **Author to whom correspondence should be addressed:** ingo.fischer@uni-wuerzburg.de

ABSTRACT

We report a joint experimental and computational study of the photoelectron spectroscopy and the dissociative photoionization of fulminic acid, HCNO. The molecule is of interest to astrochemistry and astrobiology as a potential precursor of prebiotic molecules. Synchrotron radiation was used as the photon source. Dispersive photoelectron spectra were recorded from 10 to 22 eV, covering four band systems in the HCNO cation, and an ionization energy of 10.83 eV was determined. Transitions into the Renner–Teller distorted $X^{+2}\Pi$ state of the cation were simulated using wavepacket dynamics based on a vibronic coupling Hamiltonian. Very good agreement between experiment and theory is obtained. While the first excited state of the cation shows only a broad and unstructured spectrum, the next two higher states exhibit a well-resolved vibrational progression. Transitions into the excited electronic states of $HCNO^+$ were not simulated due to the large number of electronic states that contribute to these transitions. Nevertheless, a qualitative assignment is given, based on the character of the orbitals involved in the transitions. The dissociative photoionization was investigated by photoelectron–photoion coincidence spectroscopy. The breakdown diagram shows evidence for isomerization from $HCNO^+$ to $HNCO^+$ on the cationic potential energy surface. Zero Kelvin appearance energies for the daughter ions HCO^+ and NCO^+ have been derived.

I. INTRODUCTION

Fulminic acid, HCNO, has been and still is a molecule of considerable interest in organic chemistry.[1,2] At present, the astrochemical relevance drives spectroscopic and theoretical work on the molecule because HCNO contains the basic atoms of organic chemistry. It has been detected in numerous astrophysical objects, including molecular clouds, protostars, starless cores such as B1, L1544, and L183, as well as the low-mass, star-forming region L1527.[3–8] It is most likely formed from $CH_2 + NO \rightarrow HCNO + H$ in the gas phase or $H + CNO \rightarrow HCNO$ on grains.[9,10] HCNO has three additional stable isomers: isocyanic acid (HNCO), cyanic acid (HOCN), and isofulminic acid (HONC). The relative stability is HNCO > HOCN > HCNO > HONC, with HNCO being the most stable isomer.[11] Of these molecules, only isofulminic acid has not yet been detected in interstellar space,[4] although its microwave spectrum is known.[12] Recent computational studies have also shown that HCNO and its isomers can be formed in (exo)planetary atmospheres[13] and become the simplest conceivable quaternary compounds in the high-pressure interior of Neptune-like, giant icy (exo)planets.[14] Similar

to its isomers, fulminic acid is considered to be a potential precursor in the interstellar synthesis of prebiotic molecules and might be chemically linked to small amides.[15] Laboratory astrophysics is dominated by spectroscopy in the radio frequency, microwave, and infrared. However, the availability of instruments such as the Chandra X-Ray Observatory and XMM (X-ray multi mirror)-Newton triggered interest in the interaction of molecules with high-energy vacuum ultraviolet (VUV) and soft x-ray radiation. For example, Juell *et al.* analyzed the K-shell absorption spectra of neutral and ionized atomic oxygen with Chandra.[16] Interestingly, UV and VUV radiation could also appear within dense clouds due to the so-called Prasad–Tarafdar mechanism.[17] Hydrogen molecules excited by the impact of electrons produced by cosmic-ray ionization can emit UV and VUV photons that initiate photochemistry and (dissociative) photoionization. These photons can have energies up to roughly 13.7 eV (90 nm) and influence the chemistry in dense interstellar clouds, where external UV photons may not enter. For example, the dissociation of CO to C + O and H_2O to OH + H is initiated this way.[18,19] Accurate estimation of photodissociation and dissociative photoionization is, therefore, relevant for astrochemical, gas–grain models, where the photodissociation of HCNO has so far only been estimated.[9]

Given the importance of HCNO in astrochemistry, it is not surprising that significant work has been dedicated to this molecule. Due to its small size, HCNO and its isomers have been investigated by various high-level quantum chemical approaches.[11,20–25] Bunker *et al.* used the semirigid bender Hamiltonian to fit the remarkably flat potential of the HCN bending mode,[26] which even inspired two limericks that are included in a review on quasilinear and quasiplanar molecules by Bunker.[27] Particularly relevant for the present work are studies by Mondal *et al.*[28] on the appearance of Jahn–Teller and Renner–Teller interactions in $HCNO^+$, as well as the work by Luna *et al.*, who published the global potential energy surface of the $[H, C, N, O]^+$ system using density functional theory.[29] Experimentally, the microwave[30–32] and IR-spectra[32–40] have been reported, the photodissociation has been investigated at 248 nm[41] and 193 nm,[42] and the kinetics of the HCNO + OH reaction has been studied.[43] In the soft x-ray regime, we recently reported normal and resonant Auger spectra of HCNO at all three K-edges.[44] In contrast, valence photoelectron spectra have only been reported using He I and II ionizations.[45] An adiabatic ionization energy IE_{ad} = 10.83 eV has been derived, and transitions into electronically excited states of the ion have been observed. However, band assignments were based on rather simple computations, and the Renner–Teller effect in the $X^{+2}\Pi$ ground state of $HCNO^+$ was not considered. Hop *et al.* investigated the products formed through electron impact ionization.[46] The main dissociation products were m/z 30 and m/z 27, as well as a large number of other products with smaller intensities. Due to the limitations of their setup, they were not able to provide energy selective data or provide insights into the mechanism of dissociation. In this joint experimental and computational study, we, therefore, reinvestigate the photoionization and dissociative photoionization of HCNO by photoelectron spectroscopy, using synchrotron radiation and coupled-cluster calculations. When combined with high-level computations, photoelectron spectroscopy has shown to be an excellent tool to characterize the electronic structure of reactive molecules,[47] as shown, for example, in the recent work on C_4H_4—the paradigm for antiaromaticity.[48] Note that the photoionization of the isomer isocyanic acid, HNCO, has already been extensively investigated by our group.[49,50]

II. EXPERIMENTAL AND COMPUTATIONAL METHODS

A. Experimental

The photoelectron spectrum was recorded at the soft x-ray beamline PLEIADES[51] of synchrotron SOLEIL, while the breakdown diagram for the analysis of dissociative photoionization was obtained at the VUV beamline of the Swiss Light Source (SLS) in Villigen.[52] Fulminic acid was prepared according to the procedure by Wentrup *et al.*[53] Details on the synthesis are given in the supplementary material.

At the PLEIADES beamline, the HCNO sample enters a gas cell through an effusive inlet. Here, it interacts with the synchrotron light, which is produced by an Apple II HU256 undulator and monochromatized by 400 lines mm^{-1} grating. The photon energy was fixed at 30 eV, and the light was circularly polarized. Since the undulator cannot produce light oriented at the magic angle relative to the detector at this low energy, circularly polarized light was used to avoid anisotropy of the emitted electrons. Electrons entered a VG Scienta R4000 hemispherical electron analyzer through an entrance slit of 300 μm. A pass energy of 5 eV was adjusted, leading to a spectral resolution of 6 meV. Electron binding energies E_B are obtained by subtracting the photoelectron kinetic energy from the photon energy $h\nu$:

$$E_B = h\nu - E_{kin}. \quad (1)$$

Error bars in the photoelectron spectra are derived from the full width at half maximum of the peak.

At the VUV beamline,[52] the sample also enters the experimental chamber through an effusive inlet. A bending magnet delivers the synchrotron radiation, which is monochromatized using a 150 lines mm^{-1} grating. Electrons and ions were detected in coincidence with a multi-start/multi-stop scheme by a pair of position-sensitive Roentdeck DL40 detectors with a delay line anode.[54] Threshold electrons were collected with a resolution of 5 meV, the contributions of hot electrons were subtracted according to the procedure of Sztaray and Baer.[55] The breakdown diagram is produced by dividing the threshold electron signal of each relevant mass channel by the sum of all relevant mass channels. It was recorded from 11.5 to 13.5 eV, with 25 meV step size, and from 13.5 to 15.3 eV, with 20 meV step size.

B. Computational

The equilibrium structures of neutral fulminic acid and the fulminic acid cation were calculated using Molpro[56–58] at the CCSD(T)/cc-pVTZ and RCCSD(T)/cc-pVTZ levels of theory,[59–61] respectively. Both molecules were restricted to be linear. The harmonic vibrational normal modes and frequencies were calculated at optimized geometries using the same methods.

We initially intended to simulate the full experimental photoelectron spectra of fulminic acid; however, it was found that at least 12 electronic states of the molecule spanned the energy range of experiments (see discussion in the supplementary material). The excited state potential energy surfaces were also found to vary in a complicated way along the normal mode coordinates such that they

could not be described using a vibronic coupling model. Here, we restrict the simulation of the photoelectron spectra to the first two electronic states of the fulminic acid cation.

Ab initio energies for the fulminic acid cation were calculated using OpenMolcas[62] along 1D and 2D cuts of each (neutral) normal mode from the equilibrium geometry outward, using a two state-averaged restricted active space self-consistent field[63] (RASSCF) method, followed by second order multiconfigurational perturbation theory[64,65] (CASPT2). The active space comprised 11 electrons in ten orbitals (11, 10). For the neutral molecule, a cc-pVDZ basis was used, while for the cation, a cc-pVTZ basis was employed. These calculations were based on an initial unrestricted Hartree–Fock treatment at the equilibrium geometry, and RASSCF orbitals from the previous geometry were used as starting orbitals for each subsequent geometry. Symmetry was turned off for all calculations, and a level shift of 0.2 hartree was used for CASPT2 calculations.

To obtain coupled potential energy surfaces for dynamics calculations and spectrum simulations, a vibronic coupling Hamiltonian model[66] was employed. The diabatic potentials are expressed as a Taylor series, in dimensionless (mass-frequency scaled) normal modes, around a particular point, $\mathbf{Q}_0$, here, taken as the equilibrium geometry. The Hamiltonian can be written in matrix form as

$$\mathbf{H} = \mathbf{H}^{(0)} + \mathbf{W}^{(0)} + \mathbf{W}^{(1)} + \cdots, \tag{2}$$

with the zeroth-order diagonal Hamiltonian $\mathbf{H}^{(0)}$ often expressed in the harmonic approximation

$$H_{ii}^{(0)} = \sum_{\alpha} \frac{\omega_\alpha}{2}\left(\frac{\partial}{\partial Q_\alpha^2} + Q_\alpha^2\right). \tag{3}$$

The subsequent matrices include the effects of electronic excitation and vibronic coupling as a Taylor expansion around $\mathbf{Q}_0$. The zero-order term $\mathbf{W}^{(0)}$ is a diagonal matrix of excitation energies. The first order term $\mathbf{W}^{(1)}$ usually contains on-diagonal linear terms for each electronic state and off-diagonal linear terms, coupling states along a particular mode; however, for fulminic acid, these terms are absent due to symmetry.

As discussed in the supplementary material, for all modes, the basic harmonic potential was replaced by polynomial or Morse functions, which provide more accurate fits to the *ab initio* energies and give better agreement between the calculated and experimental photoelectron spectra.

As the fulminic acid cation is a tetra-atomic linear molecule with $C_{\infty v}$ symmetry and degenerate electronic states at equilibrium, it displays the Renner–Teller (RT) effect for the pairs of degenerate vibrations $Q_{1/2}$ and $Q_{3/4}$. These modes do not have the correct symmetry to provide linear coupling ($\mathbf{W}^{(1)}$) between the electronic states, and coupling is provided through second order terms. This causes the potential energy surfaces to meet at a glancing intersection, rather than at the peak of a cone. Of the five possible Renner–Teller cases, $HCNO^+$ is an example of case (b) as defined by Lee *et al.*:[67] both curves are repulsive as a function of bending, but the two harmonic bending frequencies have the same value.

Following Worth and Cederbaum,[68] for the two pairs of degenerate vibrational modes ($Q_{1/2}$ and $Q_{3/4}$), the vibronic coupling Renner–Teller Hamiltonian can be expressed as

$$\mathbf{H} = \frac{\omega}{2}\left(Q_i^2 + Q_j^2\right) + \begin{pmatrix} -\frac{1}{2}\gamma(Q_j^2 - Q_i^2) & \gamma Q_i Q_j \\ \gamma Q_i Q_j & \frac{1}{2}\gamma(Q_j^2 - Q_i^2) \end{pmatrix}, \tag{4}$$

where ω is the degenerate vibrational frequency for the pair of modes i and j, and γ is the parameter that causes splitting of the degenerate electronic surfaces. In this work, the harmonic potential was replaced by polynomial functions, but the RT γ parameters were retained.

The RT parameter ε can be used to describe the splitting and is defined as $V^{\pm} = V_m(1 \pm \varepsilon)$, where V_m is the mean potential of the split surfaces V^+ and V^-.[69] The RT parameter can be calculated as

$$\varepsilon = \frac{V^+ - V^-}{V^+ + V^-}. \tag{5}$$

Usually only quadratic terms are considered, which, for the fitting functions used here, give $\varepsilon = 2\gamma/\beta$, where β is the quadratic term parameter (see the supplementary material).

All parameters of the vibronic coupling Hamiltonian were obtained by least-squares fitting to the CASPT2 *ab initio* energies using the VCHAM package[70] as implemented within the Quantics program suite.[71] Fits were constrained so that the degenerate electronic energies and parameters for degenerate vibrational modes remained equal. Fitted parameters and plots comparing the *ab initio* energies to the vibronic coupling model are provided in the supplementary material.

The photoelectron spectrum of fulminic acid was simulated in a manner similar to that described previously for both, cyclobutadiene[48,72] and phenol,[73] from wavepacket dynamics simulations using the MCTDH method[74] implemented in Quantics.[71] In this case, however, thermal effects were found to be important, and a thermalized density operator was propagated in place of the usual 0 K wavepacket (see the supplementary material for 0 K spectra and assignments). Propagation was done including all seven modes using a new multilayer implementation[75] of the ρ-MCTDH algorithm of Raab *et al.*[76]

The ground state nuclear density operator of neutral fulminic acid was obtained using energy relaxation[74] of an initial density operator built from harmonic oscillator eigenfunctions, thermalized to infinite temperature and propagated in imaginary time until the temperature was 300 K, the temperature of the experimental sample. A vertical excitation was then performed by placing the ground state neutral density operator on one of the two lowest electronic states of the fulminic acid cation and then propagating on these coupled states for 200 fs. The photoelectron spectrum was obtained from the Fourier transform of the autocorrelation function as

$$I(\omega) \propto \omega \int_{-\infty}^{\infty} \mathrm{d}t\, C(t) e^{i\omega t} e^{(-t/\tau)}, \tag{6}$$

where the last factor is an exponential damping term, used to simulate experimental broadening in the photoelectron spectra This phenomenological damping term accounts for missing terms in the model and experimental line broadening by convoluting the spectral

lines with a Lorentzian function. The autocorrelation function C(t) is defined as

$$C(t) = \mathrm{Re}\{\mathrm{Tr}\rho_{s0}\}, \quad (7)$$

where ρ_{s0} is the off-diagonal density matrix connecting the neutral ground-state with the initially excited cation state *s*. All seven vibrational modes were included in the calculation in a three-layer multi-layer scheme,[77] adding basis functions, until convergence with respect to the autocorrelation function was obtained. For all modes, the primitive basis functions were harmonic oscillator DVRs (discrete variable representations), with 21 points used. Assignments in the photoelectron spectra to specific vibrational modes were determined by including/excluding modes from the simulation and observing the effect on the simulated spectrum.

The mechanism of the dissociation of the fulminic acid cation was calculated using the Gaussian-4 composite method[78] contained in the Gaussian09 program.[79] The evaluated intermediates and transition states are based on the previous DFT calculations by Luna *et al.*[29] Transition states were located using the Berny algorithm.[80] They were identified by the presence of a vibration with an imaginary frequency, which corresponded to the respective reaction coordinate. The coordinates of all the intermediates and transition states are given in the supplementary material (Tables S8 and S9). With these transition states, the breakdown diagram is modeled using the minimalPEPICO program.[81]

III. RESULTS AND DISCUSSION

A. Equilibrium geometry and harmonic frequencies

Equilibrium bond lengths of r_{HC} = 1.06 (1.08), r_{CN} = 1.17 (1.17), and r_{NO} = 1.21 (1.21) Å were calculated for HCNO ($HCNO^+$), in good agreement with more elaborate calculations, for the neutral molecule.[25] Harmonic vibrational frequencies are given in Table I along with their symmetry labels (in C_{2v}). Values obtained by Mladenović and Lewerenz[25] are also given for comparison. The force vectors of the normal modes are shown in the supplementary material.

For the doubly degenerate H–C–N bend, lower levels of theory give imaginary frequencies, indicating that this geometry is not the global minimum. Many experimental[26,31,36,38,39] and theoretical[11,20–23] studies have been carried out to determine whether the equilibrium structure of fulminic acid is linear or bent. As shown by Mladenović and Lewerenz,[25] and Bunker *et al.*,[26] fulminic acid is a very floppy molecule, with an almost flat region of the potential energy surface for hydrogen bending motions. Very large basis sets are required, to converge to a linear equilibrium structure. Since we obtain cuts through the potential energy surface along the calculated normal modes, the precise determination of the equilibrium structure is not important here. As an aside, we note that in practical applications, fulminic acid is usually taken to have a linear structure, for example, in determining its electronic and magnetic properties,[82] or for describing collisions with other species.[83]

For the cation, the harmonic stretching frequencies are broadly similar to the neutral. Values for the bending modes are seen not to be degenerate, only approximately so. Although as discussed above, the fulminic acid cation displays the Renner–Teller effect for the bending modes and, thus, a simple harmonic description is not sufficient, we retain harmonic frequencies for reference purposes. From least squares fits to the CASPT2 *ab initio* energies, we obtain γ parameter values [see Eq. (4)] of 0.062959 and 0.0054112 eV for modes $\omega_{1/2}$ and $\omega_{3/4}$, respectively. Using Eq. (5), this gives RT parameters $|\varepsilon|$ of 0.48 and 0.41, respectively, indicating a somewhat intermediate coupling strength, compared to other RT systems.[69]

B. Photoelectron spectrum

Figure 1 shows the complete photoelectron spectrum. Four bands are observed at around 10.83, 16.0, 17.81 and 19.08 eV. The first, third, and fourth bands show a well-separated vibrational structure, while the second band is broad and unstructured. The spectrum agrees overall well with the previous dispersive photoelectron spectrum by Bastide and Maier;[45] however, due to the higher resolution, additional bands are observed. Several narrow transitions appear, which are assigned to ionization of H_2O and N_2. They are indicated by asterisks in Fig. 1.

Figure 2 shows the experimentally observed first band in more detail (black line); partial vibrational resolution is visible. From the first band, an IE_{ad} = 10.83 ± 0.02 eV is derived. The error bars are based on the full width of the band at half maximum. The value is in very good agreement with the previous one of 10.83 eV.[45] The main peak shows a shoulder on the high energy side, and an irregular progression of multiple peaks is observed.

The red line in Fig. 2 shows the simulated photoelectron spectra obtained from MCTDH density operator dynamics, run on the first two electronic states of the cation. The simulated spectrum has

TABLE I. Comparison of harmonic vibrational frequencies with previous theoretical values of Mladenović and Lewerenz;[25] "all" denotes that all electrons were correlated in the calculation. Units of cm^{-1} are employed.

Mode	CCSD(T)/cc-pVTZ (this work)	CCSD(T)/cc-pVQZ[25]	CCSD(T)/cc-pVQZ[25] (All)	RCCSD(T)/cc-PVTZ (cation)	Description
$\omega_{1/2}(B_{1/2})$	206i	128i	33	677/512	H–C–N bend
$\omega_{3/4}(B_{1/2})$	555	555	565	402/368	C–N–O bend
$\omega_5(A_1)$	1266	1269	1279	1140	C–N–O sym. stretch
$\omega_6(A_1)$	2276	2280	2296	1992	C–N–O asym. stretch
$\omega_7(A_1)$	3500	3493	3505	3296	C–H stretch

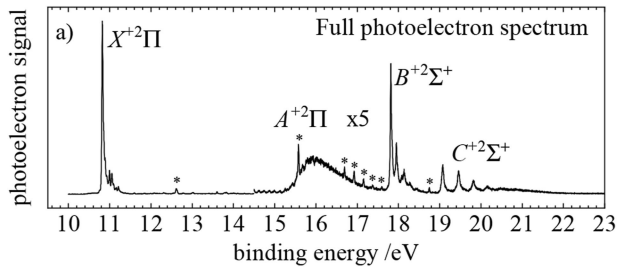

FIG. 1. Photoelectron spectrum of HCNO from 9 to 23 eV, recorded at 30 eV photon energy. The signal upward from 14.5 eV was multiplied by 5 for ease of viewing. Signals marked by asterisk are due to contamination from water (peak at 12.6 eV)[84] or molecular nitrogen (peaks at 15.6, 16.7, 16.9, 17.2, and 18.8 eV).[85]

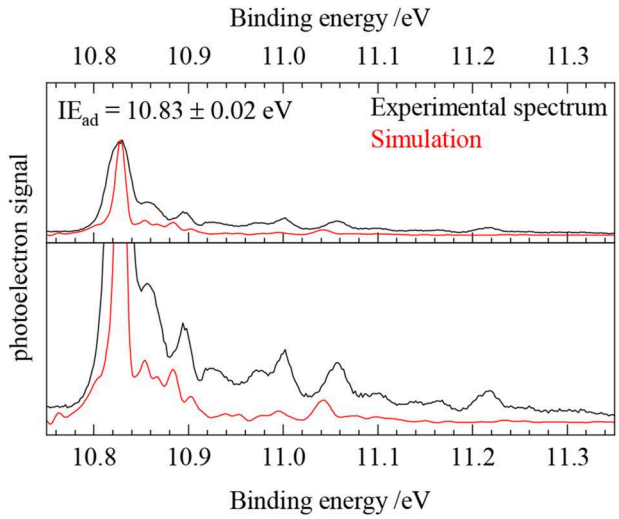

FIG. 2. Experimental photoelectron spectrum (black line), compared to the calculated spectrum (red). The simulated spectra have been normalized and shifted, to match the main peak with that of experiment.

been normalized and shifted for best agreement with experiment. To represent the experimental broadening, an exponential damping term [see Eq. (6)] was included in the computations, with a time constant of 100 fs. While the relative intensities are not fully accounted for in the simulated spectra, the peak positions in the experimental spectrum are well reproduced. To assign the spectrum, repeated runs starting at 0 K were made including different modes. Figure S12 in the supplementary material shows the full and assigned 0 K spectra, compared to the one calculated at 300 K and the experimental spectrum. The simulations show that the first peak on the main band at 10.9 eV is caused by the carbon–nitrogen–oxygen (CNO) bending modes ω_3 and ω_4. There is a small peak just below 11 eV, which is due to the CNO symmetric stretching mode ω_5. The two peaks at 11 and 11.05 eV are due to the RT modes ω_1 and ω_2 (approximate HCN bending), respectively. At higher energies, there are some smaller peaks caused by stretching modes ω_6 and ω_7 (asymmetric CNO stretch and C–H stretch, respectively). A comparison between the 0 and 300 K spectra shows that the shoulder on the high energy side of the main band is due to temperature, allowing extra transitions in the $\omega_1 - \omega_4$ vibrations.

The second band, corresponding to the A^+ state of $HCNO^+$, ranges from 15.2 to 17.6 eV and is unstructured. A close-up is shown in the supplementary material (Fig. S2). The third band is shown in Fig. 3(a). It features the intense origin band of the B^+ state at 17.81 eV and two further bands at +1130 and +2100 cm^{-1} above the origin. Additionally, a shoulder of around 240 cm^{-1} is visible for each band. The origin of the fourth band system [C^+ state, Fig. 3(b)] lies at 19.08 eV. A well-resolved progression with a spacing of around 3000 cm^{-1} is apparent.

As mentioned above, a simulation of these progressions was not possible using the vibronic coupling model. However, a tentative assignment of the progressions is provided by investigating the involved orbitals. In Fig. S4, the calculated MOs of $HCNO^+$ are shown. According to Bastide and Maier, the configuration of the neutral HCNO is $\ldots 6\sigma^2 7\sigma^2 1\pi^4 2\pi^4$.[45] For the B^+ state, they assigned two vibrational bands, with 1070 and 2420 cm^{-1} to ω_s (CNO) and ω_{as} (CNO), respectively. In our spectrum, a progression better described by a single mode is observed, so, we assign it to the symmetric CNO stretch ω_5, with a wavenumber of 1130 cm^{-1} in the excited state. This assignment is substantiated by the $2\sigma^*$ orbital (Fig. S4), corresponding to the 7σ orbital in the notation of Bastide *et al.*, which has strong CNO antibonding character. Thus, removal of an electron from this MO is expected to lead to vibrational activity in a CNO mode.

The C^+ state shows a vibrational progression with 3150 cm^{-1} for the $v^+ = 1 \leftarrow v = 0$ fundamental. Transitions into the first and second overtones at 6050 and 8630 cm^{-1}, respectively, are visible. Due to anharmonicity, the energy difference between the peaks decreases. The high vibrational wavenumber indicates that the bands have to be assigned to a progression in the C–H-stretch mode ω_7 (CH). The 2σ

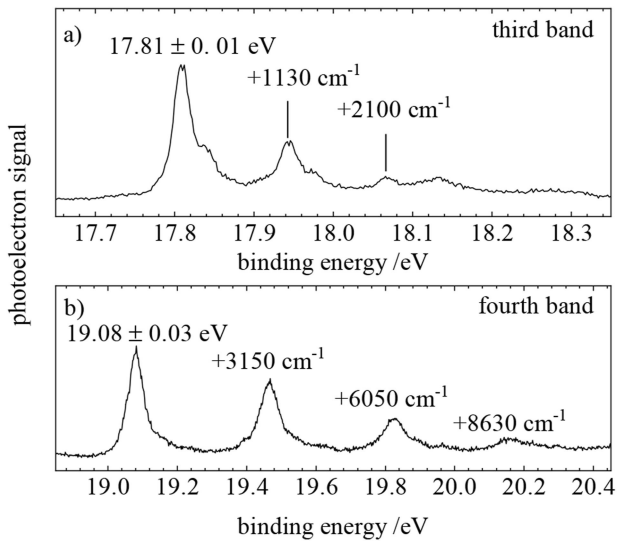

FIG. 3. High-resolution spectra of the two excited states of HCNO, with vibrational progression. (a) shows in black, the spectrum corresponding to the third band, and (b) shows the spectrum of the fourth band. The observed peaks are labeled with wavenumbers relative to the most intense peak.

MO (Fig. S4, 6σ in Bastides notation[45]) has C–H bonding character, so, a removal of that electron may destabilize the C–H bond and lead to vibrational activity in ω (CH). Nevertheless, it should be kept in mind that a simple Koopmans-type picture provides only a rather approximate description of the electronic structure that is not fully appropriate for HCNO.

C. Dissociative photoionization

The breakdown diagram for the dissociative photoionization of HCNO, recorded between 11.5 and 15.3 eV, is shown in Fig. 4. The fractional abundances of the parent and daughter ions' threshold photoelectron (TPE) signal are plotted as a function of the photon energy. The open symbols represent experimental data. The simultaneously recorded TOF distribution shows a small asymmetry for the daughter ion peaks, which indicates the presence of a kinetic shift (see Fig. S3). As we consider the effect of the kinetic shift on the thermochemical quantities determined in the present work to be small, we did not include it in the data analysis.

The breakdown diagram shows several unusual features that are in contrast with a simple sequential dissociation in the ion. Until around 12.7 eV, no fragmentation is visible, and then the signal of m/z 29 (▽) increases, which corresponds to HCO^+, while the parent signal (□) drops to zero. At 13.45 eV, m/z 42 (○) starts to rise, maximizes at around 14 eV, and decreases again. Interestingly, the rise and decrease of m/z 42 are rather slow compared to HCO^+. At this point, it is important to realize that the structure of m/z 42 is ambiguous and could correspond to CNO^+ or NCO^+. Table II shows the heats of reaction $\Delta_R H^\circ$ of the most relevant fragment channels. They are calculated using the heats of formation provided by the Active Thermochemical Tables (ATcT).[87] Assuming a barrierless mechanism, these reaction enthalpies are equivalent to appearance energies. In any case, $\Delta_R H^\circ$ represents the minimum energy that is required to produce these ions. In fact, HCO^+ appears above the computed value of 11.68 eV. The heat of reaction for formation of CNO^+ + H, the presumed carrier of m/z = 42, is $\Delta_R H^\circ$ = 16.11 eV, outside the energy range monitored in Fig. 4. However, for the product channel $^3NCO^+ + {}^2H$, $\Delta_R H^\circ$ = 13.54 eV is computed, a thermochemical value that agrees well with the observed

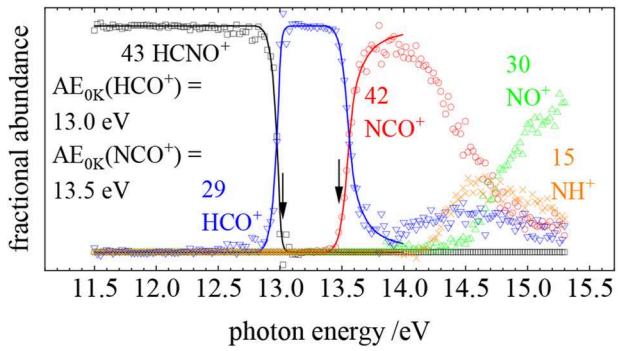

FIG. 4. Breakdown diagram of HCNO from 11.5 to 15.3 eV. The open symbols correspond to the experimental data, while the solid lines are the fit produced by the minimalPEPICO program. The labeling of the curves shows the m/z value, as well as the assigned structure. The arrows show the appearance energies produced by the fit, which are also shown on the left.

TABLE II. Heats of reaction, $\Delta_R H^\circ$ for the dissociation HCNO → products. A more extensive table is available in the supplementary material. The energies are taken from the Active Thermochemical Tables.[86] Ground state multiplicities are taken from Ref. 29.

Products	$\Delta_R H^\circ$/eV
$^1HCO^+ + {}^4N$	11.68
$^3NCO^+ + {}^2H$	13.54
$^2NH^+ + {}^1CO$	14.24
$^1NO^+ + {}^2CH$	14.57
$^3CNO^+ + {}^2H$	16.11

onset. We, therefore, conclude an isomerization on the ionic potential energy surface. The second unusual feature corresponds to the HCO^+ curve (▽), which drops to almost zero at 13.9 eV, but rises again to a value of around 12% of its maximum at 14.5 eV. This suggests two different channels for the formation of this fragment. Two more fragments are visible, the formation of m/z = 15 (×), corresponding to NH^+ at 14.1 eV, and the onset of m/z = 30 NO^+ (△) around 14.5 eV. Both fragment ion curves are in accordance with the values in Table II.

The minimalPEPICO program allows the modeling of these breakdown diagrams to extract thermochemical data.[81] This requires detailed knowledge of the reaction mechanism that forms the products and the vibrational frequencies of the stationary points of the potential energy surface. Luna *et al.* published the global potential energy surface of the $[H, N, C, O]^+$ system in doublet and quartet multiplicity, including transition states. Their findings yield the mechanism shown in Fig. 5, which was confirmed by our own calculations that yielded the necessary frequencies. The appearance of HCO^+ requires the formation of a C–O bond that is not present in the parent $HCNO^+$. This bond can form via **TS1,** where the C–N–O angle is decreased to 97.6°, which leads to the structure **I**. Formation of HCO^+ also produces atomic nitrogen. The ground state of N is $^4S^\circ_{3/2}$.[88] Since the parent ion is of doublet multiplicity, the direct formation of $HCO^+ + {}^4N$ is not possible, and the cation has to switch to the quartet surface since the product channel $HCO^+ + {}^2N$ lies at 14.1 eV. We propose that this happens either at **I,** or between **I** and the products. On the quartet, surface **I** may dissociate over **TS2** and the molecule–ion complex **II**.[29] Note that in the experiment, we only measure the highest barrier along the reaction coordinate. This mechanism can also explain the revival of HCO^+ at around 14.0 eV. At this energy, the reaction along the doublet surface is possible, to form $HCO^+ + {}^2N$ (Fig. 5) via **TS3** and the $HCON^+$ intermediate.[29] The formation of NCO^+ requires the formation of the isocyanic acid cation $HNCO^+$. This mechanism involves a 1,2-H-shift (**TS4**) to **III** and an N–O bond cleavage (**TS5**). The solid lines in Fig. 4 represent the fit obtained using the MinimalPEPICO program, employing the highest barriers (TS1 to $HCO^+ + {}^2N$ and TS4 to $NCO^+ + {}^2H$) of the above mechanism. As visible, the behavior of m/z 29 and the onset of m/z 42 are well represented. The zero Kelvin appearance energies for both fragments are derived from the model, $AE_{0\,K}$(HCNO, HCO^+) = 13.0 ± 0.1 eV and $AE_{0\,K}$(HCNO, NCO^+) = 13.5 ± 0.1 eV. The reaction coordinate for the formation of NO^+ and NH^+ has not been investigated; consequently their appearance energies are not modeled in this work. The observed onset of NCO^+ agrees very well

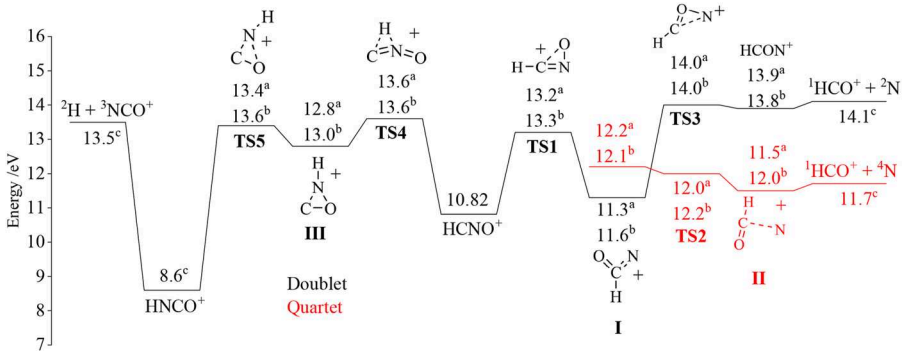

FIG. 5. Mechanism of the isomerization of the HCNO cation, to form $^3NCO^+$ and $^1HCO^+$. Energies are given in eV, relative to the neutral HCNO molecule. Values marked with [a] were calculated using the G4 composite method. Values marked with [b] and [c] were taken from Ref. 29 and from the Active Thermochemical Tables,[86] respectively. Lines shown in black are on the doublet surface, and lines in red are on the quartet surface.

with the ATcT value, while the $AE_{0\,K}$(HCNO, HCO^+) is associated with a complex doublet–quartet intersystem crossing. This ISC may be close to **TS1** or **I** (Fig. 5), and does not allow an extraction of the $\Delta_R H^\circ$.

IV. CONCLUSION

The VUV spectroscopy of fulminic acid, HCNO, has been investigated using synchrotron radiation and dispersive, as well as threshold photoelectron detection. Compared to a previous spectrum,[45] the present spectra are better resolved and show more information. Four bands are observed; three of them exhibit a vibrational progression. The band origins are identified at 10.83 ± 0.02 eV ($X^{+2}\Pi$) 17.81 ± 0.01 eV (B^+) and 19.08 ± 0.03 eV (C^+), respectively. A simulation of the transition into the Renner–Teller distorted $X^{+2}\Pi$ ground state of the cation using wavepacket dynamics that rely on a vibronic coupling Hamiltonian yielded very good agreement with the experiment. Several bending mode transitions are identified in the simulations. In addition, hot and sequence band transitions from low energy bending modes of neutral HCNO are essential to achieve agreement between experiment and simulation. No simple description of the transitions into excited electronic states of the cation is possible, because 12 electronic states contribute to the transitions, and the excited state potential energy surfaces depend, in a complicated way, on the normal mode coordinates. Therefore, only an approximate character was assigned to the transitions, which can, nevertheless, qualitatively explain the observed vibronic transitions.

Furthermore, a breakdown diagram of HCNO up to 15.3 eV was recorded to investigate its dissociative photoionization. The spectrum was then modeled, to extract thermochemical data, and the mechanism has been investigated computationally. Dissociative ionization to $^1HCO^+ + {}^4N$ was found to be the lowest energy dissociation pathway, with an appearance energy of $AE_{0\,K}$(HCNO, HCO^+) = 13.0 ± 0.1 eV. The reaction requires a switch to the quartet potential energy surface in the cation. Next, dissociation to $^3NCO^+ + {}^2H$ sets in at $AE_{0\,K}$(HCNO, NCO^+) = 13.5 ± 0.1 eV. This dissociation is preceded by an isomerization from $HCNO^+$ to $HNCO^+$, which proceeds via a tricyclic intermediate. The confirmation of isomerization from $HCNO^+$ to $HNCO^+$ might be relevant for explaining the relative abundance of the various CHNO isomers in space and their fragments, which is not well understood.[89]

SUPPLEMENTARY MATERIAL

See the supplementary material for additional experimental and computational information.

ACKNOWLEDGMENTS

The photoelectron spectra were recorded at the PLEIADES beamline at Synchrotron SOLEIL, France, Proposal No. 20200183. We thank E. Robert for technical assistance and the SOLEIL staff for operation of the equipment and storage ring during the experiments. The dissociative photoionization was investigated at the VUV beamline of the Swiss Light Source, Villigen/CH. This work was funded by the Deutsche Forschungsgemeinschaft, Contract No. FI575/13-2. B.P.M. and G.W. acknowledge financial support from the UK Engineering and Physical Science Research Council (EPSRC), Grant No. EP/T006560/1.

AUTHOR DECLARATIONS

Conflict of Interest

The authors have no conflicts to disclose.

Author Contributions

Marius Gerlach: Formal analysis (equal); Investigation (lead); Methodology (equal); Writing – original draft (equal). **Barry Mant**: Formal analysis (equal); Investigation (equal); Writing – original draft (equal). **Tobias Preitschopf**: Investigation (supporting). **Emil Karaev**: Investigation (supporting). **Dennis Mayer**: Investigation (supporting). **Heidy M. Quitián-Lara**: Investigation (supporting). **Patrick Hemberger**: Formal analysis (supporting); Investigation (supporting); Methodology (equal); Resources (equal); Supervision (supporting); Writing – review & editing (supporting). **John Bozek**: Conceptualization (supporting); Formal analysis (supporting); Investigation (supporting); Methodology (equal); Resources (equal); Writing – review & editing (supporting). **Graham Worth**: Formal analysis (equal); Funding acquisition (equal); Methodology (equal); Project administration (equal); Supervision (equal); Writing – review & editing (equal). **Ingo Fischer**: Conceptualization (lead); Funding acquisition (lead); Investigation (supporting); Methodology (equal); Project administration (equal); Resources (equal); Supervision (equal); Writing – review & editing (equal).

DATA AVAILABILITY

The data that support the findings of this study are available within the article and its supplementary material. Further data are available from the authors upon request.

REFERENCES

[1] F. Kurzer, J. Chem. Educ. **77**, 851 (2000).
[2] C. Wentrup, Angew. Chem., Int. Ed. **58**, 14800 (2019).
[3] N. Marcelino, J. Cernicharo, B. Tercero, and E. Roueff, Astrophys. J. **690**, L27 (2009).
[4] N. Marcelino, S. Brünken, J. Cernicharo, D. Quan, E. Roueff, E. Herbst, and P. Thaddeus, Astron. Astrophys. **516**, A105 (2010).
[5] E. Mendoza, B. Lefloch, A. López-Sepulcre, C. Ceccarelli, C. Codella, H. M. Boechat-Roberty, and R. Bachiller, Mon. Not. R. Astron. Soc. **445**, 151 (2014).
[6] B. Lefloch, R. Bachiller, C. Ceccarelli, J. Cernicharo, C. Codella, A. Fuente, C. Kahane, A. López-Sepulcre, M. Tafalla, C. Vastel, E. Caux, M. González-García, E. Bianchi, A. Gómez-Ruiz, J. Holdship, E. Mendoza, J. Ospina-Zamudio, L. Podio, D. Quénard, E. Roueff, N. Sakai, S. Viti, S. Yamamoto, K. Yoshida, C. Favre, T. Monfredini, H. M. Quitián-Lara, N. Marcelino, H. M. Boechat-Roberty, and S. Cabrit, Mon. Not. R. Astron. Soc. **477**, 4792 (2018).
[7] N. Marcelino, M. Agúndez, J. Cernicharo, E. Roueff, and M. Tafalla, Astron. Astrophys. **612**, L10 (2018).
[8] M. Agúndez, N. Marcelino, J. Cernicharo, E. Roueff, and M. Tafalla, Astron. Astrophys. **625**, A147 (2019).
[9] D. Quan, E. Herbst, Y. Osamura, and E. Roueff, Astrophys. J. **725**, 2101 (2010).
[10] S. Brünken, A. Belloche, S. Martín, L. Verheyen, and K. M. Menten, Astron. Astrophys. **516**, A109 (2010).
[11] M. S. Schuurman, S. R. Muir, W. D. Allen, and H. F. Schaefer III, J. Chem. Phys. **120**, 11586 (2004).
[12] M. Mladenović, M. Lewerenz, M. C. McCarthy, and P. Thaddeus, J. Chem. Phys. **131**, 174308 (2009).
[13] K. Molaverdikhani, T. Henning, and P. Mollière, Astrophys. J. **883**, 194 (2019).
[14] L. J. Conway, C. J. Pickard, and A. Hermann, Proc. Natl. Acad. Sci. U. S. A. **118**, e2026360118 (2021).
[15] P. Gorai, B. Bhat, M. Sil, S. K. Mondal, R. Ghosh, S. K. Chakrabarti, and A. Das, Astrophys. J. **895**, 86 (2020).
[16] A. M. Juett, N. S. Schulz, and D. Chakrabarty, Astrophys. J. **612**, 308 (2004).
[17] S. S. Prasad and S. P. Tarafdar, Astrophys. J. **267**, 603 (1983).
[18] R. Gredel, S. Lepp, A. Dalgarno, and E. Herbst, Astrophys. J. **347**, 289 (1989).
[19] A. Sternberg, A. Dalgarno, and S. Lepp, Astrophys. J. **320**, 676 (1987).
[20] M. T. Nguyen, K. Pierloot, and L. G. Vanquickenborne, Chem. Phys. Lett. **181**, 83 (1991).
[21] A. P. Rendell, T. J. Lee, and R. Lindh, Chem. Phys. Lett. **194**, 84 (1992).
[22] N. Pinnavaia, M. J. Bramley, M.-D. Su, W. H. Green, and N. C. Handy, Mol. Phys. **78**, 319 (1993).
[23] J. Koput, B. P. Winnewisser, and M. Winnewisser, Chem. Phys. Lett. **255**, 357 (1996).
[24] A. M. Mebel, A. Luna, M. C. Lin, and K. Morokuma, J. Chem. Phys. **105**, 6439 (1996).
[25] M. Mladenović and M. Lewerenz, Chem. Phys. **343**, 129 (2008).
[26] P. R. Bunker, B. M. Landsberg, and B. P. Winnewisser, J. Mol. Spectrosc. **74**, 9 (1979).
[27] P. R. Bunker, Annu. Rev. Phys. Chem. **34**, 59 (1983).
[28] R. Mondal and D. Debasis Mukhopadhyay, Int. J. Quantum Chem. **120**, e26195 (2020).
[29] A. Luna, A. M. Mebel, and K. Morokuma, J. Chem. Phys. **105**, 3187 (1996).
[30] M. Winnewisser and H. K. Bodenseh, Z. Naturforsch., A **22**, 1724 (1967).
[31] B. P. Winnewisser, M. Winnewisser, and F. Winther, J. Mol. Spectrosc. **51**, 65 (1974).
[32] B. P. Winnewisser, M. Winnewisser, G. Wagner, and J. Preusser, J. Mol. Spectrosc. **142**, 29 (1990).
[33] W. Beck and K. Feldl, Angew. Chem. **78**, 746 (1966).
[34] B. P. Winnewisser and M. Winnewisser, J. Mol. Spectrosc. **29**, 505 (1969).
[35] W. Beck, P. Swoboda, K. Feldl, and R. S. Tobias, Chem. Ber. **104**, 533 (1971).
[36] E. L. Ferretti and K. Narahari Rao, J. Mol. Struct. **51**, 97 (1974).
[37] V. E. Bondybey, J. H. English, C. W. Mathews, and R. J. Contolini, J. Mol. Spectrosc. **92**, 431 (1982).
[38] B. P. Winnewisser and P. Jensen, J. Mol. Spectrosc. **101**, 408 (1983).
[39] S. Albert, M. Winnewisser, and B. P. Winnewisser, Ber. Bunsenges. **100**, 1876 (1996).
[40] S. Albert, K. K. Albert, M. Winnewisser, and B. P. Winnewisser, J. Mol. Struct. **599**, 347 (2001).
[41] W. Feng and J. F. Hershberger, J. Phys. Chem. A **118**, 829 (2014).
[42] W. Feng and J. F. Hershberger, Chem. Phys. **472**, 18 (2016).
[43] W. Feng, J. P. Meyer, and J. F. Hershberger, J. Phys. Chem. A **110**, 4458 (2006).
[44] M. Gerlach, T. Preitschopf, E. Karaev, H. M. Quitián-Lara, D. Mayer, J. Bozek, I. Fischer, and R. F. Fink, Phys. Chem. Chem. Phys. **24**, 15217 (2022).
[45] J. Bastide and J. P. Maier, Chem. Phys. **12**, 177 (1976).
[46] C. E. C. A. Hop, K. J. Van den Berg, J. L. Holmes, and J. K. Terlouw, J. Am. Chem. Soc. **111**, 72 (1989).
[47] I. Fischer and S. T. Pratt, Phys. Chem. Chem. Phys. **24**, 1944 (2022).
[48] L. Bosse, B. P. Mant, D. Schleier, M. Gerlach, I. Fischer, A. Krueger, P. Hemberger, and G. Worth, J. Phys. Chem. Lett. **12**, 6901 (2021).
[49] F. Holzmeier, M. Lang, I. Fischer, X. Tang, B. Cunha de Miranda, C. Romanzin, C. Alcaraz, and P. Hemberger, J. Chem. Phys. **142**, 184306 (2015).
[50] F. Holzmeier, T. J. A. Wolf, C. Gienger, I. Wagner, J. Bozek, S. Nandi, C. Nicolas, I. Fischer, M. Gühr, and R. F. Fink, J. Chem. Phys. **149**, 034308 (2018).
[51] See https://www.synchrotron-soleil.fr/fr/lignes-de-lumiere/pleiades for a detailed description of the beamline, 2019.
[52] M. Johnson, A. Bodi, L. Schulz, and T. Gerber, Nucl. Instrum. Methods Phys. Res., Sect. A **610**, 597 (2009).
[53] C. Wentrup, B. Gerecht, and H. Briehl, Angew. Chem., Int. Ed. **18**, 467 (1979).
[54] B. Sztáray, K. Voronova, K. G. Torma, K. J. Covert, A. Bodi, P. Hemberger, T. Gerber, and D. L. Osborn, J. Chem. Phys. **147**, 013944 (2017).
[55] B. Sztáray and T. Baer, Rev. Sci. Instrum. **74**, 3763 (2003).
[56] H.-J. Werner, P. J. Knowles, G. Knizia, F. R. Manby, and M. Schütz, Wiley Interdiscip. Rev.: Comput. Mol. Sci. **2**, 242 (2012).
[57] H.-J. Werner, P. J. Knowles, G. Knizia, F. R. Manby, M. Schütz *et al.*, Molpro, Version 2019.2, a package of *ab initio* programs (2019), see https://www.molpro.net.
[58] H.-J. Werner, P. J. Knowles, F. R. Manby, J. A. Black, K. Doll, A. Heßelmann, D. Kats, A. Köhn, T. Korona, D. A. Kreplin, Q. Ma, T. F. Miller III, A. Mitrushchenkov, K. A. Peterson, I. Polyak, G. Rauhut, and M. Sibaev, J. Chem. Phys. **152**, 144107 (2020).
[59] M. J. O. Deegan and P. J. Knowles, Chem. Phys. Lett. **227**, 321 (1994).
[60] T. H. Dunning, Jr., J. Chem. Phys. **90**, 1007 (1989).
[61] J. D. Watts, J. Gauss, and R. J. Bartlett, J. Chem. Phys. **98**, 8718 (1993).
[62] I. Fdez Galván, M. Vacher, A. Alavi, C. Angeli, F. Aquilante, J. Autschbach, J. J. Bao, S. I. Bokarev, N. A. Bogdanov, R. K. Carlson, L. F. Chibotaru, J. Creutzberg, N. Dattani, M. G. Delcey, S. S. Dong, A. Dreuw, L. Freitag, L. M. Frutos, L. Gagliardi, F. Gendron, A. Giussani, L. González, G. Grell, M. Guo, C. E. Hoyer, M. Johansson, S. Keller, S. Knecht, G. Kovačević, E. Källman, G. Li Manni, M. Lundberg, Y. Ma, S. Mai, J. P. Malhado, P. Å. Malmqvist, P. Marquetand, S. A. Mewes, J. Norell, M. Olivucci, M. Oppel, Q. M. Phung, K. Pierloot, F. Plasser, M. Reiher, A. M. Sand, I. Schapiro, P. Sharma, C. J. Stein, L. K. Sørensen, D. G. Truhlar, M. Ugandi, L. Ungur, A. Valentini, S. Vancoillie, V. Veryazov, O. Weser, T. A. Wesołowski, P.-O. Widmark, S. Wouters, A. Zech, J. P. Zobel, and R. Lindh, J. Chem. Theory Comput. **15**, 5925 (2019).
[63] P. A. Malmqvist, A. Rendell, and B. O. Roos, J. Phys. Chem. **94**, 5477 (1990).
[64] P. Å. Malmqvist, K. Pierloot, A. R. M. Shahi, C. J. Cramer, and L. Gagliardi, J. Chem. Phys. **128**, 204109 (2008).
[65] V. Sauri, L. Serrano-Andrés, A. R. M. Shahi, L. Gagliardi, S. Vancoillie, and K. Pierloot, J. Chem. Theory Comput. **7**, 153 (2011).

[66]H. Köppel, W. Domcke, and L. S. Cederbaum, Adv. Chem. Phys. **57**, 59 (1984).
[67]T. J. Lee, D. J. Fox, H. F. Schaefer III, and R. M. Pitzer, J. Chem. Phys. **81**, 356 (1984).
[68]G. A. Worth and L. S. Cederbaum, Annu. Rev. Phys. Chem. **55**, 127 (2004).
[69]Q. Lu, ACS Omega **7**, 44078 (2022).
[70]G. A. Worth, K. Giri, G. W. Richings, I. Burghardt, M. H. Beck, A. Jäckle, and H.-D. Meyer, The Quantics Package Version2.0. See http://www.chem.ucl.ac.uk/quantics, University College London, UK, 2020.
[71]G. A. Worth, Comput. Phys. Commun. **248**, 107040 (2020).
[72]S. Saddique and G. A. Worth, Chem. Phys. **329**, 99 (2006).
[73]M. P. Taylor and G. A. Worth, Chem. Phys. **515**, 719 (2018).
[74]M. H. Beck, A. Jäckle, G. A. Worth, and H.-D. Meyer, Phys. Rep. **324**, 1 (2000).
[75]A. Van Haeften, C. Ash, and G. A. Worth, J. Chem. Phys. (2023) (unpublished).
[76]A. Raab, I. Burghardt, and H. D. Meyer, J. Chem. Phys. **111**, 8759 (1999).
[77]O. Vendrell and H.-D. Meyer, J. Chem. Phys. **134**, 044135 (2011).
[78]L. A. Curtiss, P. C. Redfern, and K. Raghavachari, J. Chem. Phys. **126**, 084108 (2007).
[79]M. J. Frisch, G. W. Trucks, H. B. Schlegel, G. E. Scuseria, M. A. Robb, J. R. Cheeseman, G. Scalmani, V. Barone, B. Mennucci, G. A. Petersson, H. Nakatsuji, M. Caricato, X. Li, H. P. Hratchian, A. F. Izmaylov, J. Bloino, G. Zheng, J. L. Sonnenberg, M. Hada, M. Ehara, K. Toyota, R. Fukuda, J. Hasegawa, M. Ishida, T. Nakajima, Y. Honda, O. Kitao, H. Nakai, T. Vreven, J. A. Montgomery, Jr., J. E. Peralta, F. Ogliaro, M. Bearpark, J. J. Heyd, E. Brothers, K. N. Kudin, V. N. Staroverov, R. Kobayashi, J. Normand, K. Raghavachari, A. Rendell, J. C. Burant, S. S. Iyengar, J. Tomasi, M. Cossi, N. Rega, J. M. Millam, M. Klene, J. E. Knox, J. B. Cross, V. Bakken, C. Adamo, J. Jaramillo, R. Gomperts, R. E. Stratmann, O. Yazyev, A. J. Austin, R. Cammi, C. Pomelli, J. W. Ochterski, R. L. Martin, K. Morokuma, V. G. Zakrzewski, G. A. Voth, P. Salvador, J. J. Dannenberg, S. Dapprich, A. D. Daniels, Ö. Farkas, J. B. Foresman, J. V. Ortiz, J. Cioslowski, and D. J. Fox, GAUSSIAN 16, Revision B.01, Gaussian, Inc., Wallingford CT, 2016).
[80]H. B. Schlegel, J. Comput. Chem. **3**, 214 (1982).
[81]B. Sztáray, A. Bodi, and T. Baer, J. Mass Spectrom. **45**, 1233 (2010).
[82]M. Mladenović, M. Elhiyani, and M. Lewerenzc, J. Chem. Phys. **131**, 034302 (2009).
[83]A. Naindouba, C. Nkem, Y. Ajili, K. Hammami, N. Gotoum, and L. C. Owono Owono, Chem. Phys. Lett. **636**, 67 (2015).
[84]J. E. Reutt, L. S. Wang, Y. T. Lee, and D. A. Shirley, J. Chem. Phys. **85**, 6928 (1986).
[85]J. W. Rabalais, T. P. Debies, J. L. Berkosky, J. T. J. Huang, and F. O. Ellison, J. Chem. Phys. **61**, 516 (1974).
[86]B. Ruscic and D. H. Bross, Active Thermochemical Tables (ATcT) values based on ver. 1.122r of the Thermochemical Network (2021), available at https://ATcT.anl.gov.
[87]B. Ruscic, R. E. Pinzon, G. v. Laszewski, D. Kodeboyina, A. Burcat, D. Leahy, D. Montoy, and A. F. Wagner, J. Phys.: Conf. Ser. **16**, 561 (2005).
[88]A. Kramida, Yu. Ralchenko, J. Reader, and NIST ASD Team, NIST Atomic Spectra Database (ver. 5.9) (2021), available: https://physics.nist.gov/asd, 2022, August 31, National Institute of Standards and Technology, Gaithersburg, MD.
[89]A. Jiménez-Escobar, B. M. Giuliano, G. M. M. Caro, J. Cernicharo, and N. Marcelino, Astrophys. J. **788**, 19 (2014).